Arresting aqueous swelling of layered graphene-oxide membranes with H_3O^+ and OH^- ions

Arresting Aqueous Swelling of Layered Graphene-Oxide Membranes with H_3O^+ and OH^- Ions

Abhijit Gogoi,[*,†,‡] Erik C. Neyts,[*,†,¶] Milorad V. Milošević,[*,‡,¶] and François M. Peeters[*,‡]

†*PLASMANT, Department of Chemistry, University of Antwerp, 2610 Antwerp, Belgium.*
‡*Department of Physics, University of Antwerp, 2020 Antwerp, Belgium.*
¶*NANOlab Center of Excellence, University of Antwerp, Belgium.*

E-mail: abhijit.gogoi@uantwerpen.be; erik.neyts@uantwerpen.be;
milorad.milosevic@uantwerpen.be; francois.peeters@uantwerpen.be

Abstract

Over the past decade, graphene oxide (GO) has emerged as a promising membrane material with superior separation performance and intriguing mechanical/chemical stability. However, its practical implementation remains very challenging primarily due to its undesirable swelling in aqueous environment. Here we demonstrated that dissociation of water molecules into H_3O^+ and OH^- ions inside the interlayer gallery of layered GO membrane can strongly affect its stability and performance. We reveal that H_3O^+ and OH^- ions form clusters inside the GO laminates that impede permeance of water and salt ions through the membrane. Dynamics of those clusters is sensitive to an external *ac* electric field, which can be used to tailor the membrane performance. The presence of H_3O^+ and OH^- ions also leads to increased stability of the hydrogen bond (H-bond) network among the water molecules and the GO layers, which further reduces water permeance through the membrane, while crucially imparting stability to layered GO membrane against undesirable swelling.

KEYWORDS: *layered graphene-oxide membrane, aqueous stability, H_3O^+ and OH^- ions, external electric field, molecular dynamics*

1 Introduction

Over the last decade, there have been extensive studies on graphene-based membranes such as single and multi layered graphene,[1,2] carbon nanotube (CNT)[3] and graphene oxide (GO),[4–6] which revealed their superior water flux with intriguing mechanical and chemical stability. Porous monolayer graphene was attributed with water permeability several orders of magnitude higher than conventional reverse osmosis (RO) membranes ($\approx 2\mathrm{Lm^{-2}h^{-1}bar^{-1}}$)[7,8] with exceptional salt rejection (almost 100%). Unfortunately, industrial scale production of atomically thin membranes and creating high-density nanopores on them without affecting the mechanical rigidity is technologically very challenging. On the other hand, layered GO membranes are highly scalable and are compatible with presently available membrane-based technologies. Consequently, they rapidly gain enormous interest from the research community.[9–14] Driven by the extensive research over the years, GO has emerged as a highly potent alternative to conventional membrane materials for a wide range of applications such as sea water desalination,[15,16] water purification,[17,18] ion sieving,[19,20] molecular separation,[21,22] gas sensing[23,24] etc.

While dried GO laminates are completely impermeable to gas and liquids[5], the hydrated GO laminates get rapidly intercalated by several layers of water.[6,25] This can be attributed to the strong interaction of the oxygen-containing functional groups with water. While this phenomenon facilitates water transport, it often leads to swelling of layered GO membranes in aqueous environment which can significantly deteriorate its performance.[26,27] Because of this, smaller ions (ions with hydrated radii < 4.5 Å) can easily pass through the layered GO membranes.[4]

In recent years, a number of strategies have been suggested to address the issue of undesirable aqueous swelling of layered GO membrane or to tune its interlayer spacing. These strategies include partial reduction of the GO nanosheets,[28,29] using external cross-linker for GO nanosheets,[30,31] electrochemical oxidation,[19] intercalating large nanomaterials,[32,33] nitrogen doping,[34] physical confinement of the GO laminates,[20,35] chemical modifications and external pressure regulations[36,37] etc. However, these strategies have certain functional drawbacks which limits their use in layered GO membranes for practical applications. For example, the partial reduction of the GO nanosheets significantly lowers the water flux. This also severely affects the surface hydrophilicity and antifouling properties of the membrane.[38] Similarly, the use of external cross-linkers and intercalating nanomaterials may result in lower water flux[39] and some of them show little rejection for smaller ions.[40,41] Construction of these nanomaterials is also a difficult task. Along with this, maintaining the stability of these types of membranes and their scalability is also quite challenging.[42–44]

Recently, it was suggested that intercalating the GO laminates with cations such as K^+, Li^+, Na^+, Mg^{2+}, Ca^{2+} etc. could impart aqueous stability to layered GO membranes against swelling.[45,46] They can also be used to tune the interlayer spacing of layered GO membranes. However, intercalating layered GO membranes with such cations is not suited for water purification applications, as exactly these cations deemed to be rejected from the feed solution. However, following the same idea, one can consider the generation of H_3O^+ ions inside the interlayer gallery of layered GO membranes under the influence of external electric field. Recently, Zhou *et al.*[47] demonstrated the idea of electrically controlled water permeation through layered GO membranes with experimental and theoretical studies where they reported the clustering of H_3O^+/OH^- ions inside the membrane. Applying an external electric field could also improve the performance of graphene-based membranes.[48,49] In fact, in micro and nanoscale regime, fluid transport can be effectively and easily controlled by the application of an external electric field. Also, coupling electric field to the conventional pressure driven processes for separation and purification applications will provide additional degrees of freedom to effectively control the transport process.

In the present study, we have investigated the performance of layered GO membranes under the influence of an external electric field. As the water molecules can get dissociated into H_3O^+ and OH^- ions under the influence of an external electric field, we consider the presence of H_3O^+ and OH^- ions inside the interlayer gallery of layered GO membranes. We use molecular dynamics (MD) simulation to gain detailed atomistic insights into various factors. The effect of the presence of H_3O^+/OH^- ions and the external electric field on the water and salt dynamics is reported in detail in subsequent sections. These factors also significantly influence the internal structure of a layered GO membrane, which is a crucial parameter in determining its performance.

2 Methodology

To prepare the simulation setup for our MD simulations, we first constructed the layered GO membranes. For this, GO nanosheets of two different sizes are constructed using Visual Molecular Dynamics (VMD)[50] and Avogadro[51] as shown in Fig 1(a). The sizes of the GO nanosheets are 39×48 Å^2 and 31×48 Å^2. The chemical composition of the GO nanosheets is $C_{10}O_1(OH)_1(COOH)_{0.5}$.[52–56] In

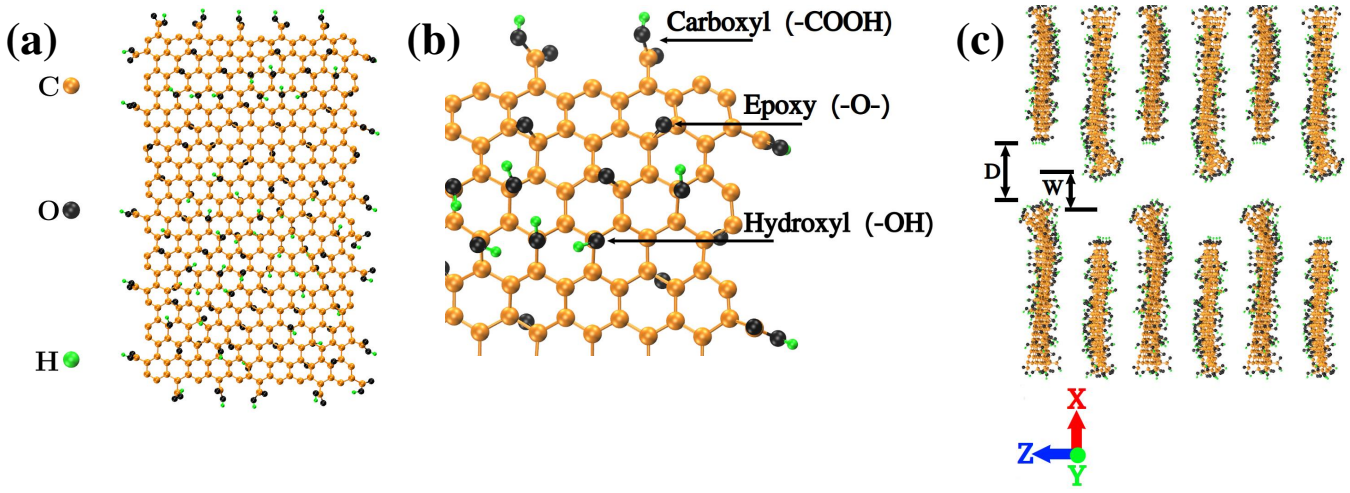

Figure 1: (a) GO nanosheet. (b) Typical functional groups on a GO nanosheet. (c) Layered GO membrane as considered in this work.

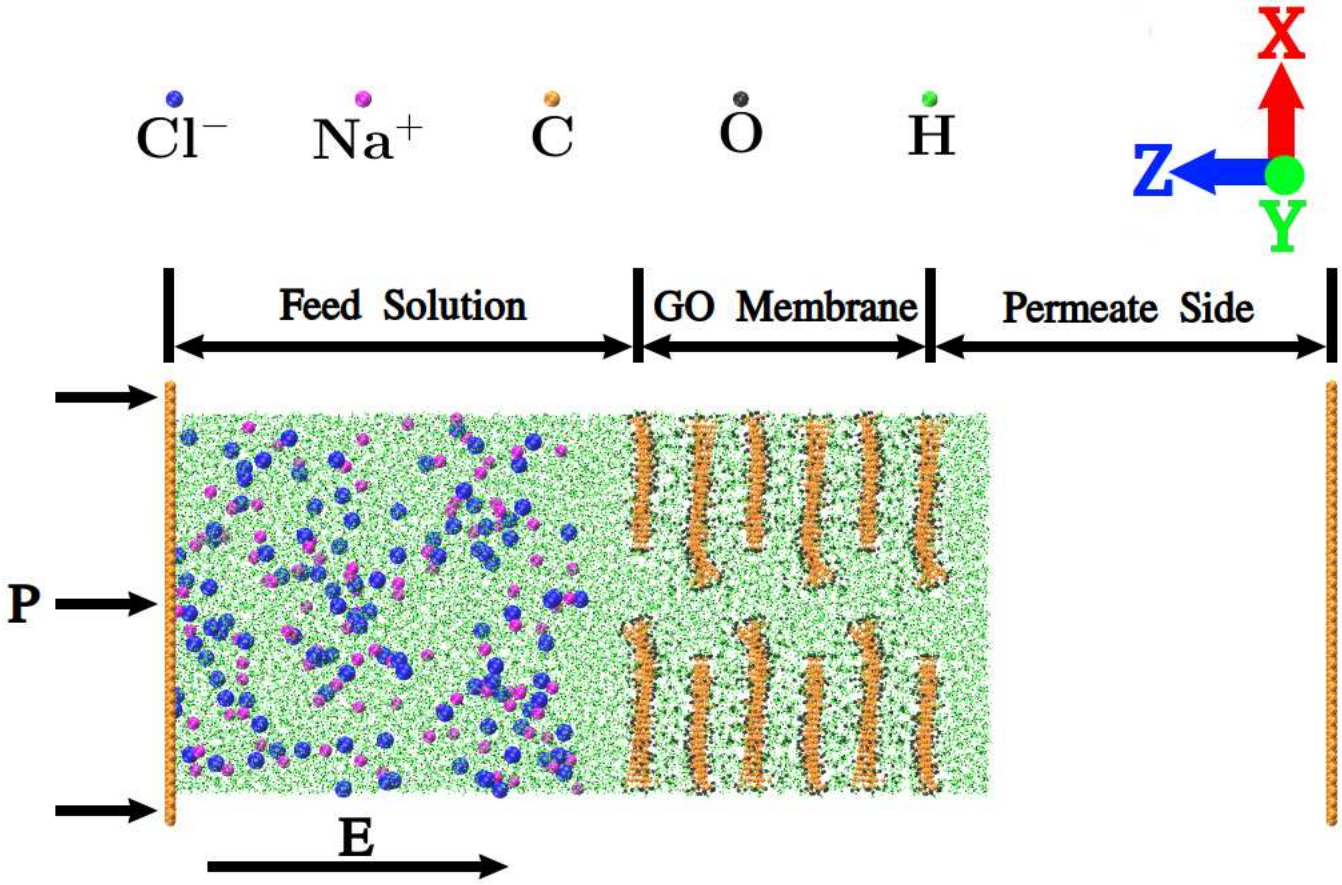

Figure 2: Simulation setup. The feed solution of Na^+ and Cl^- ions is pressed through the layered GO membrane, in the presence of an external electric field as depicted.

the GO nanosheets, the epoxy and hydroxyl groups are located on the basal plane while the carboxyl groups are located at the edges[52,53] (Fig. 1(b)). These GO nanosheets are arranged in space to construct the layered GO membrane as shown in Fig. 1(c). In Fig. 1(c), the parameters **D**, **W** and **H** are the geometric parameters of the membrane known as pore width, pore

offset distance and interlayer distance, respectively. In the present study, the values of **D**, **W** and **H** are 12 Å, 8 Å and 12 Å, respectively. To study the effect of H_3O^+/OH^- ions on the performance of layered GO membranes, three different cases of water dissociation are considered as follows:

- Pure: no water molecule is dissociated.
- 3%: 3% of the water molecules are dissociated into H_3O^+ and OH^- ions inside the interlayer gallery of layered GO membranes.
- 10%: 10% of the water molecules are dissociated into H_3O^+ and OH^- ions inside the interlayer gallery of layered GO membranes.

The membrane is first hydrated with an equilibrated water box. The H_3O^+/OH^- ions are then randomly placed inside the interlayer gallery of the hydrated layered GO membrane and subsequently equilibrated at a constant temperature of 300 K and at a constant pressure of 1 atm. A 0.56 M aqueous NaCl solution is considered as the feed solution to mimic the sea water osmotic pressure (about 27 atm). It contains 10^4 water molecules, 108 Na^+ ions and 108 Cl^- ions. The simulation setup is shown in Fig. 2. A graphene piston is used to apply a transmembrane pressure **P** on the feed solution, and **E** is the applied external electric field. Both **P** and **E** are applied along $-Z$ direction. We considered **P** as 50 MPa, which seems quite large as compared to the transmembrane pressure used in practical applications. However, in typical MD simulations it is a common practice to use large transmembrane pressure to get sufficient water permeation in the short simulation time, mainly limited by the computational cost.[57–59] The external electric field **E** used in this work is an oscillating *ac* field given by $\mathbf{E} = \mathbf{E}_0 \cos(\omega t - \phi)$. Here $\mathbf{E}_0$ is the amplitude, ω is the frequency, and ϕ is the phase at the initial time step. The used value of $\mathbf{E}_0$ is 0.1 $^{V}/_{Å}$ which is seemingly high for real world applications but is often used in MD simulations to yield better signal-to-noise ratio.[48] The values of ω and ϕ are 0.005 fs^{-1} and 90°, respectively. Simulations are performed for sole reverse osmosis (**RO**) and reverse osmosis assisted by an external electric field (**RO+E**). On the permeate side, a graphene sheet is placed as a reservoir wall which is fixed in space during the course of the simulations.

To perform the MD simulations, NAMD 2.14[60] package is used with OPLS-AA force field parameters.[61] Water molecules are modeled using the SPC water model.[62] The bond lengths of the water molecules are constrained using SETTLE algorithm.[63] The van der Waals interactions are computed using Lennard-Jones potential with a cut-off distance of 12 Å. For the computation of the long range electrostatic interactions, Particle mesh Ewald (PME) method[64] is used.

Each of the simulation system is first energy minimized and then subsequently equilibrated for 2 ns at a constant temperature of 300 K and at a constant pressure of 1 atm. For controlling the pressure, modified Nosé-Hoover method is used with a barostat oscillation time and damping factor of 0.3 ps. Temperature is controlled using Langevin dynamics with a damping factor of 5 ps^{-1}. Finally, production runs are performed for 20 ns at a constant temperature of 300 K. During the production runs, the GO nanosheets (except at the top and bottom of the membrane) are constrained in the XY plane while they are free to move along the Z direction. The corner C atoms of the GO nanosheets located at the top and bottom of the membrane are fixed in space, so that membrane boundaries can be clearly distinguished. Periodic boundary conditions (PBC) are applied along all the directions. Along Z direction, an empty space (vacuum) of 50 Å in length is applied both at the top and bottom of the simulation system. For each of the simulation system, 3 independent simulations are performed, each with different initial configurations. The results are then averaged over these 3 independent simulations.

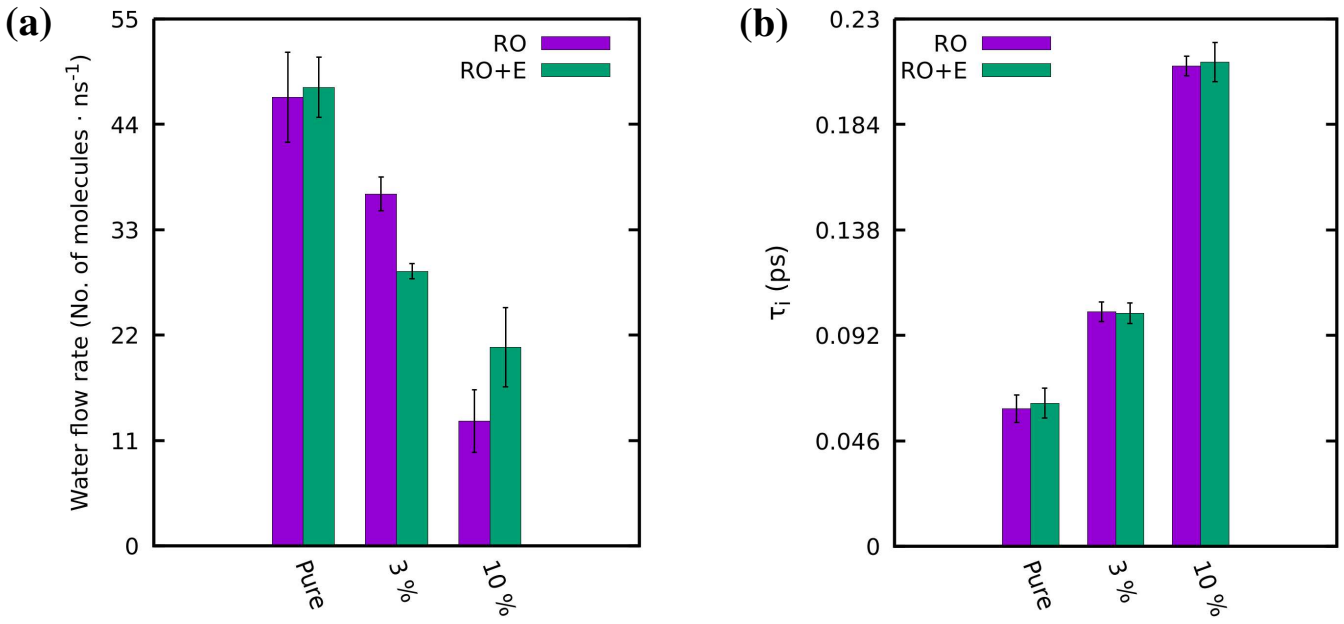

Figure 3: (a) Rate of water permeance through layered GO membranes. (b) Intermittent H-bond lifetime between water molecules and the GO nanosheets.

3 Results and discussion

From our MD simulations, first we computed the water permeance through the layered GO membranes. We start from the number of water molecules which permeate through the membrane from the feed solution to the permeate side (N_{FP}). Although the net driving force is along the $-Z$ direction, i.e. from the feed solution to the permeate side, because of the thermal motions, a few water molecules have found their way from the permeate side to the feed solution (N_{PF}). The water permeance is then calculated as the difference between N_{FP} and N_{PF} (i.e. water permeance = $N_{FP} - N_{PF}$). Fig. 3(a) shows the rate of water permeance through layered GO membranes for different cases. It is observed that water permeance is highest for the Pure case followed by the cases of 3% and 10% water dissociation. This observation is in accordance with the observation reported by Zhou *et al.*[47] As in Ref. 47, we also observed that H_3O^+/OH^- ions form clusters inside the interlayer gallery of layered GO membranes which impedes the water permeation through the membranes. This clustering can be attributed to the strong hydrogen bonding (H-bond) between H_3O^+/OH^- ions as shown in Fig. S1 of the supporting information. For the 10% case, this clustering is more prominent which leads to the lowest water permeance. However, we observed that apart from this clustering of H_3O^+/OH^- ions, there is another significant cause of this difference in water permeance, which is the stability of the H-bond between water molecules and the GO nanosheets. Also, it is found that the external electric field influences the water permeance through layered GO membranes for each of the cases independently (i.e. Pure, 3% and 10%). This will be discussed in the subsequent section.

The lifetime of the H-bond is calculated from the long time decay of the following autocorrelation function:[65]

$$C_{\mathrm{k}}(t) = \frac{< h_{ij}(t_0)\, h_{ij}(t_0 + t) >}{h_{ij}(t_0)^2} \cong \exp\{-\frac{t}{\tau_{\mathrm{k}}}\}, \quad (1)$$

where

$$h_{ij}(t) = \begin{cases} 1 & \text{If there is a H-bond between molecules i and j at times } t_0 \text{ and } t, \text{ and the bond has not been broken for any period longer than } t^*; \\ 0 & \text{Otherwise.} \end{cases}$$

The limiting cases $t^* = 0$ and $t^* = \infty$, correspond to continuous ($C_{\mathrm{c}}(t)$) and intermittent ($C_{\mathrm{i}}(t)$) H-bond autocorrelation function, respectively ($k = c$ for continuous and $k = i$ for intermittent H-bond autocorrelation functions). Considering the complexity of the simulation system, in the present study, we consider the lifetime of H-bond computed from the intermittent H-bond autocorrelation function (τ_{i}). However, the qualitative trend for the continuous H-bond autocorrelation would be the same. Fig. 3(b) shows the H-bond lifetime between water molecules and the GO nanosheets. For the 10% case, the H-bond between water molecules and the GO nanosheets are most stable (or strong) followed by the 3% case and the Pure case. This is also observed from the H-bond dynamics reported in the supporting information (Figs. S2-S4). Because of this stable H-bond between water molecules and the GO nanosheets, there is lowest permeation of water molecules for the 10% case followed by the 3% and Pure cases as observed in Fig. 3(a). Notice that the external electric field has very little impact on the H-bond lifetime between the water molecules and the GO nanosheets, as can be seen from Fig. 3(b).

The difference in the stability of H-bond between water molecules and the GO nanosheets for different cases can be attributed to the water orientational relaxation dynamics ($\mathbf{C_e}$). It gives an idea about how fast water molecules are rotating/changing directions. A fast decay of $\mathbf{C_e}$ signifies that the water molecules are rotating/changing directions rapidly. $\mathbf{C_e}$ is a time correlation function calculated as follows:[66]

$$\mathbf{C_e} = < P_2[\,\vec{e}(t_0) \cdot \vec{e}(t_0 + t)\,] > \qquad (2)$$

where $\vec{e}$ is the unit vector along the dipole vector and P_2 is the second-order Legendre polynomial. Figures 4(a) and 4(b) show the water orientational relaxation dynamics ($\mathbf{C_e}$) inside the interlayer gallery of layered GO membranes for the **RO** and **RO+E** cases, respectively. It is observed that the presence of H_3O^+/OH^- ions significantly affects $\mathbf{C_e}$ inside the interlayer gallery of layered GO membranes. With the presence of H_3O^+/OH^- ions, the water molecules rotate/change directions very slowly, which facilitates stronger (or more stable) H-bond network between water molecules and GO nanosheets. This slow rotation of the water molecules is caused by the clustering of the H_3O^+/OH^- ions and interactions of the water molecules with H_3O^+/OH^- ions as reported in the supporting information (Fig. S5). This effect is more prominent for the 10% case followed by the 3% and Pure cases. It is also observed that the external electric field used in this study has very little influence on $\mathbf{C_e}$, as shown in Fig. S6 of the supporting information. However, an electric field with significantly higher frequency does influence $\mathbf{C_e}$, as shown in Figs. S15, S16 and S17 of the supporting information.

The external electric field and the presence of H_3O^+/OH^- ions also significantly influence the internal structure of the layered GO membrane. To investigate this, we computed the **pore size distribution** (PSD) of the membrane. However, it should be noted that PSD is not directly related to **W** (Fig. 1(c)), although the terminology looks similar. **W** is a geometric parameter of the membrane, while PSD shows how much vacant space (or voids) are available inside a membrane for the water/ions/impurities to permeate through. Here, PSD is calculated using the method proposed by Bhattacharya and Gubbins.[67] Pore size at a given point of a model structure can be defined as the largest sphere that encompasses the given point without overlapping the neighboring wall atoms. For the calculation of PSD, first a cumulative histogram $C(D)$ is constructed, where $C(D)$ represents the probability of finding a point inside the model structure with a pore size larger than or equal to D. Then PSD is

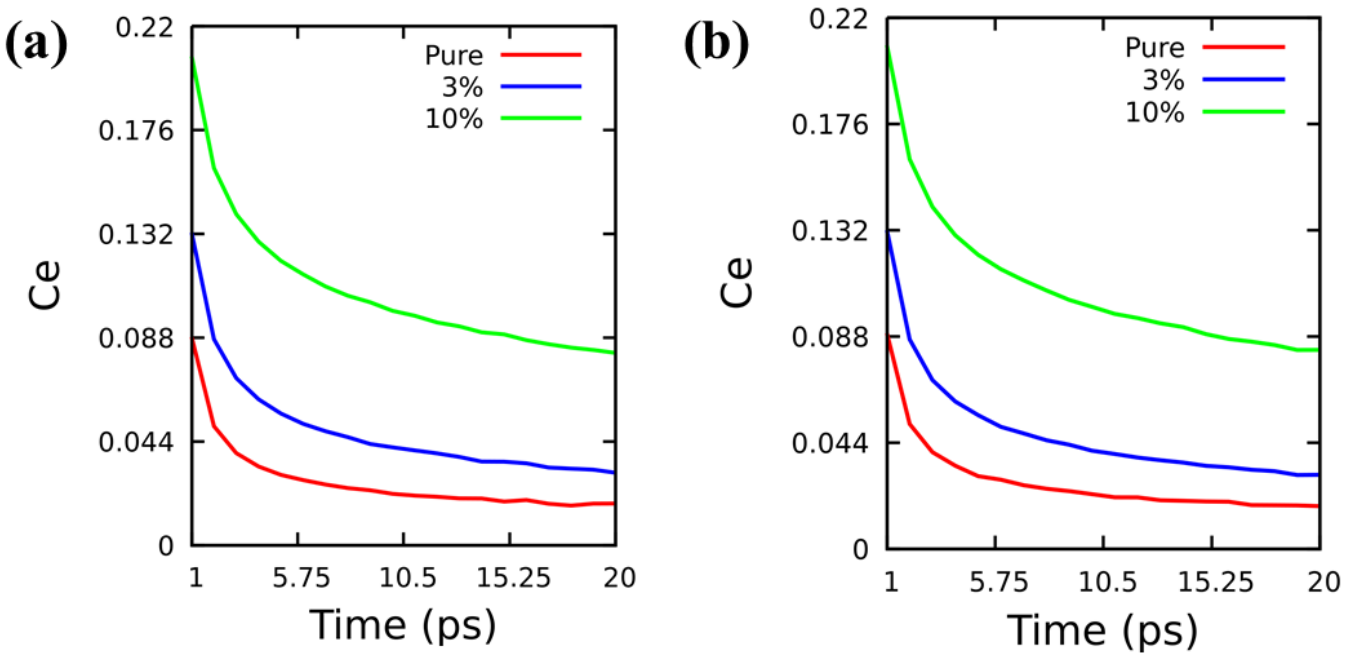

Figure 4: Water orientational relaxation dynamics ($\mathbf{C_e}$) inside the interlayer gallery of layered GO membranes, in cases of (a) **RO**, and (b) **RO+E** for different degree of dissociations of water molecules.

calculated as

$$PSD(D) = -\frac{\mathrm{d}C(D)}{\mathrm{d}D} \tag{3}$$

Figs. 5(a) and 5(b) show the $C(D)$ for **RO** and **RO+E** cases, respectively. Similarly, Figs. 5(c) and 5(d) show the PSD for these respective cases. Notice that the presence of H_3O^+/OH^- ions leads to a decrease in pore sizes both in the lower and the upper ranges of the pore size distribution. However, it leads to an increase in the pore size in the middle range. The decrease in the larger pore size of layered GO membranes in the presence of H_3O^+/OH^- ions signifies that *these ions can arrest swelling of layered GO membranes in aqueous environment*. This finding can clearly be attributed to the stronger H-bond between the water molecules and the GO nanosheets in the presence of H_3O^+/OH^- ions. The effect of H-bonding is evident from the fact that the water molecules located close to the H_3O^+/OH^- ions form stronger H-bond with GO nanosheets as compared to water molecules located away from the H_3O^+/OH^- ions as shown in Fig. 6.

Along with higher water flux, the ability of a membrane to reject undesirable impurities/ions is also important. Typically, a good quality membrane should have high water flux with low salt/impurity permeability (i.e. high rejection). However, there is a trade-off between these two qualities depending on specific applications. Considering the limited timescale of the MD simulations, it is challenging to get statistically noise-free sampling of the ion permeation through the membranes. So, to compare the rejection ability (or ion permeance) of different layered GO membranes, we consider the amount of ions that are intercalated inside the membrane during the course of the simulation. Figs. 7(a) and 7(b) show the observed rate of ion intercalation inside layered GO membranes for Cl^- and Na^+ ions, respectively. With the increase in the water dissociation, layered GO membrane become more impermeable to both Cl^- and Na^+ ions as can be seen from Figs. 7(a) and 7(b), respectively. This can be attributed to the clustering of H_3O^+/OH^- ions inside the membrane. Along with this, stability of H-bond between the water molecules and the GO nanosheets also influences the per-

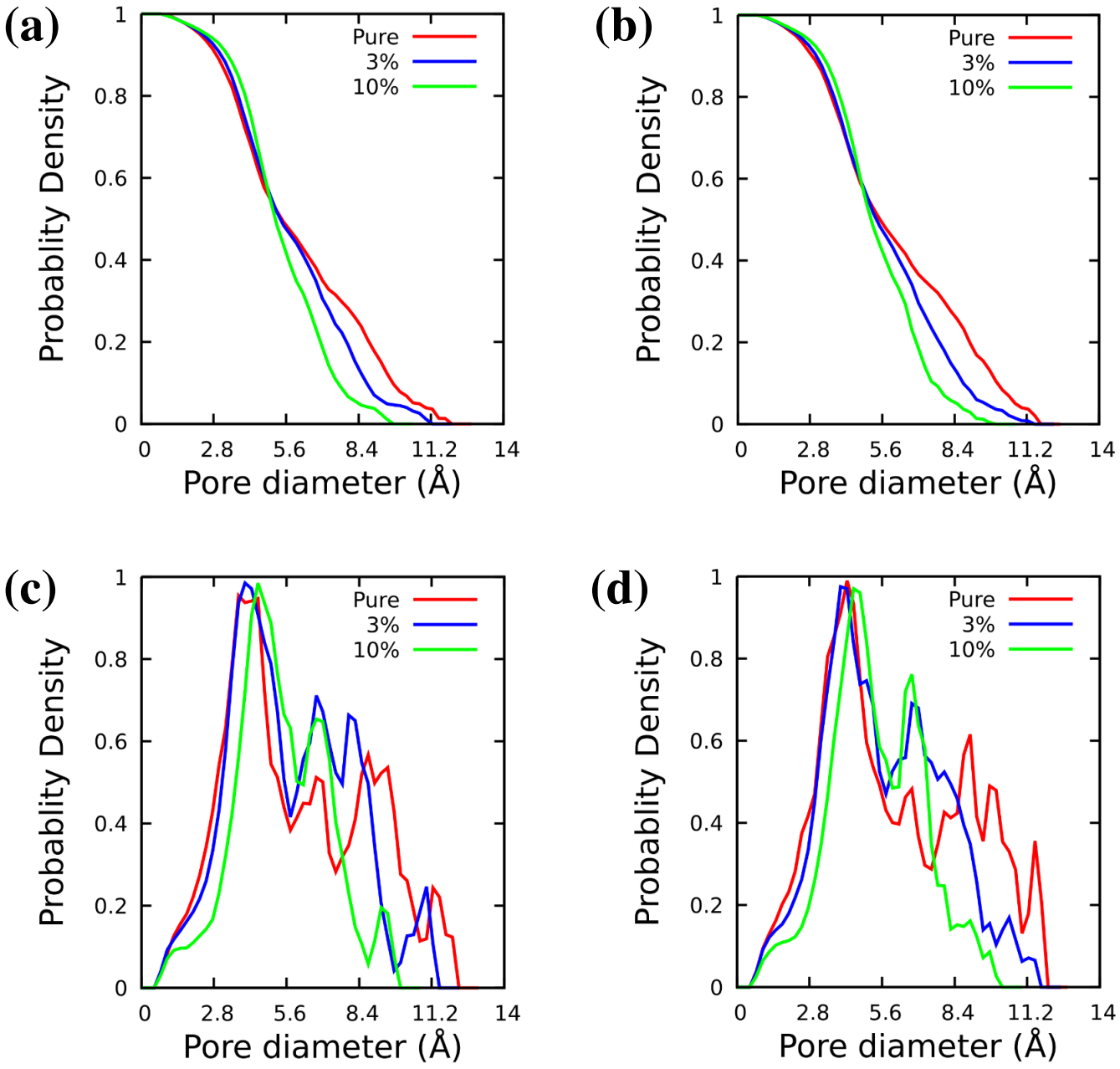

Figure 5: (a), (b) $C(D)$ and (c), (d) PSD for layered GO membranes. (a), (c) for **RO** and (b), (d) for **RO+E** case.

meability of Na^+ and Cl^- ions. With the increase in the number of H_3O^+/OH^- ions, the H-bonding between the GO nanosheets and the water molecules located in the hydration shell of Na^+/Cl^- ions become more stable (Fig. S10). As a consequence, Na^+/Cl^- ions find it difficult to permeate inside the membrane. With the application of external electric field, the permeability of Cl^- ions through layered GO membranes increases. This is due to the fact that the external electric field is applied along the $-Z$ direction i.e. from the feed solution to the permeate side, which assists the permeation of Cl^- ions. On the other hand, the permeability of Na^+ ions through the layered GO membranes follows the trend as dictated by the applied direction of external electric field for the Pure and 3% cases. On the contrary, for the 10% case, application of external electric field leads to the increase in the permeation of Na^+ ions, to be explained in what follows.

As observed in Fig. 3(a), for the Pure case,

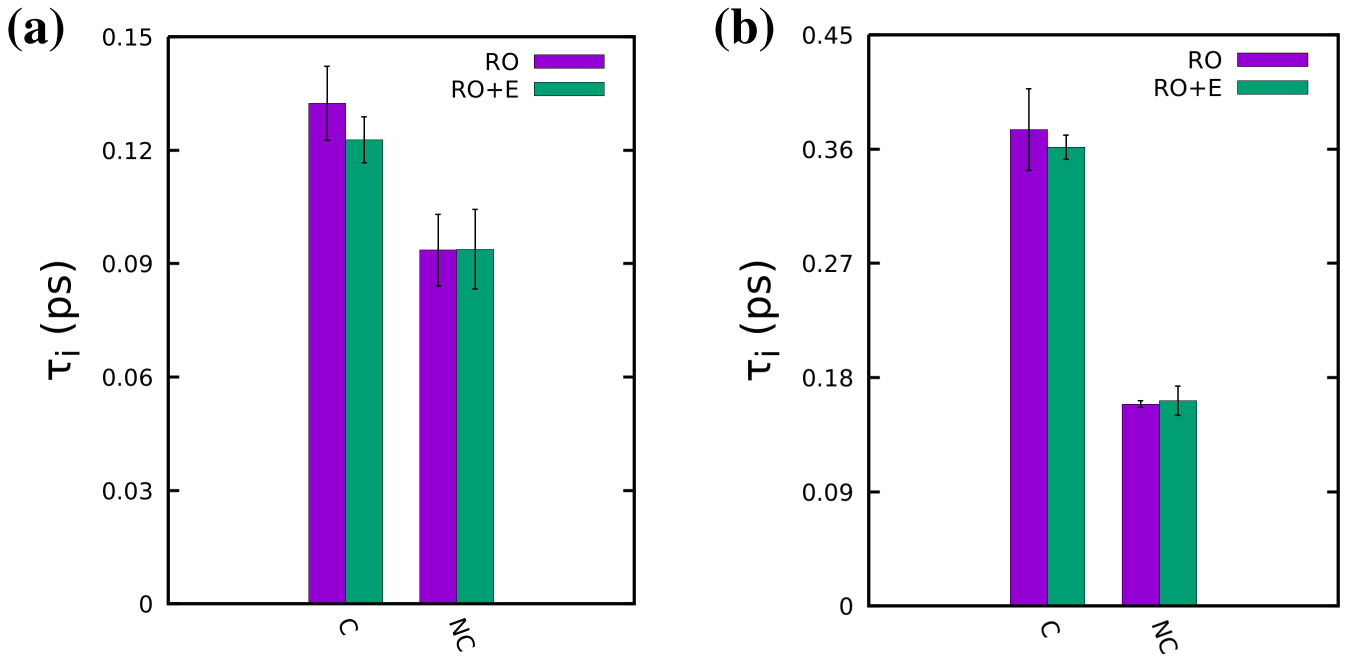

Figure 6: H-bond lifetime between GO nanosheets and water molecules located close (C) to the H_3O^+/OH^- ions and away (NC) from the H_3O^+/OH^- ions: (a) 3% case, (b) 10% case.

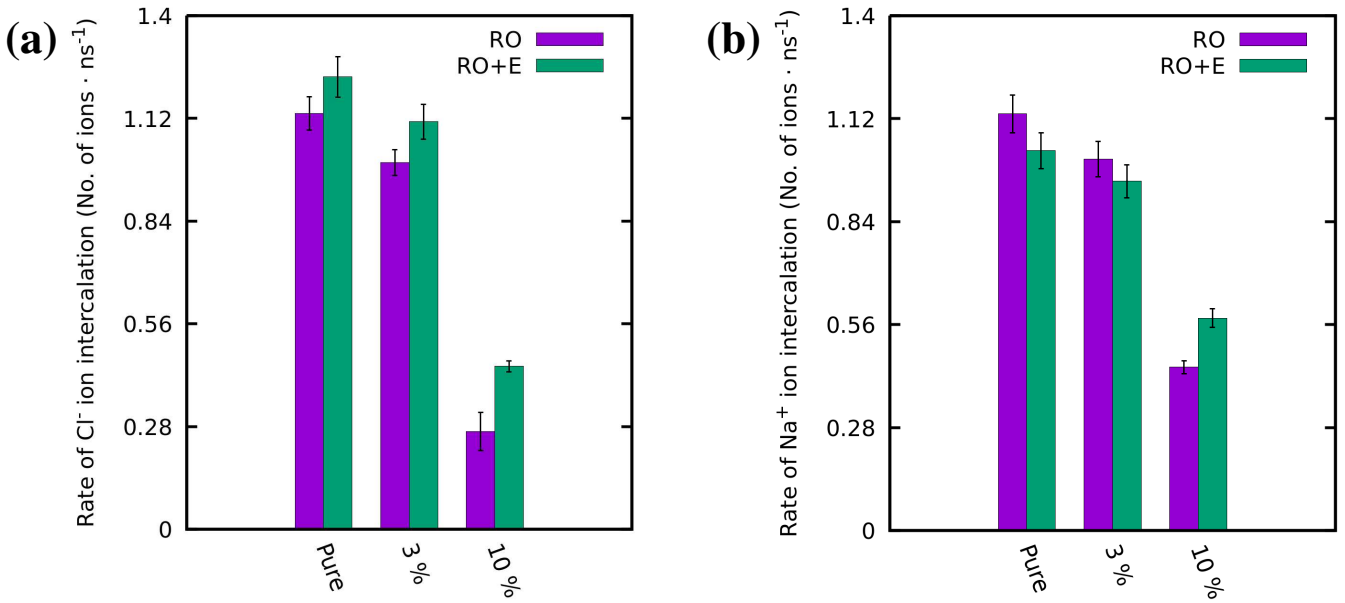

Figure 7: Rate of ion intercalation inside the layered GO membrane (a) Cl^-, and (b) Na^+ ions.

water permeance through layered GO membrane is slightly higher in the presence of external electric field. This is due to the fact that the application of external electric field increases the pore sizes of the membrane as shown in Fig. 8. Under the influence of the external electric field, the GO nanosheets fluctuate more and pores become effectively larger. This increase in fluctuations of the GO nanosheets is caused by the presence of partial positive and negative charges on the GO nanosheets owing to the presence of the oxygen containing functional groups. Along with this, the directional movement of the Na^+ and Cl^- ions under the influ-

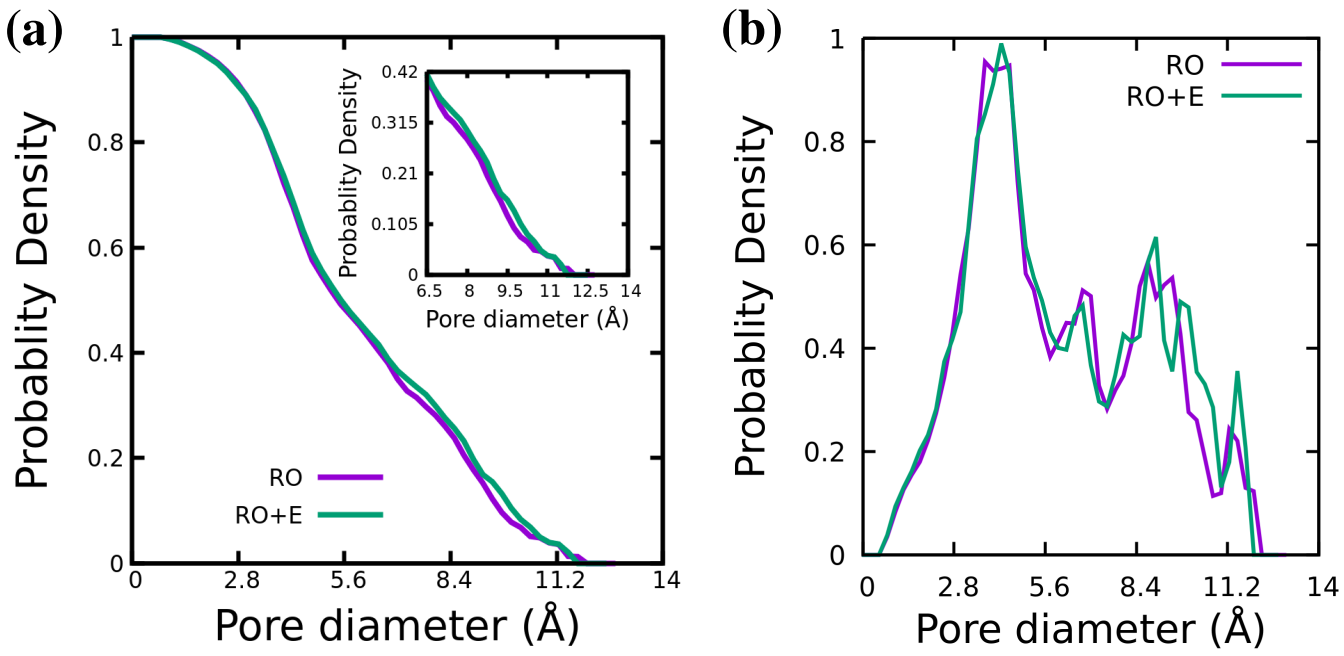

Figure 8: (a) $C(D)$, (b) PSD for the Pure case.

ence of external electric field also contributes to the fluctuations of the GO nanosheets. To get an quantitative estimate of the increase in the pore sizes we computed the area under the PSD curve. The area under the PSD curve represents the probability of finding a pore size within that region. However, it should also be noted that with reference to Eq. 3, the area under the PSD curve between 2 points D_1 and D_2 is simply $C(D_1) - C(D_2)$. For Fig. 8(b), the area under the curve for **RO** is 4% lower than **RO+E**. For the 3% water dissociation case, the water permeance decreases with the application of an external electric field (Fig. 3(a)). To get further insight into this, we need to calculate $C(D)$ and PSD considering the clustering of H_3O^+/OH^- ions. Figs. 9(a) and 9(b) show the $C(D)$ and PSD, respectively, for the 3% case considering the clustering of H_3O^+/OH^- ions. From Fig. 9, it can be seen that the application of external electric field decreases the number of larger pores (> 8 Å) for the membrane. Here again, to get a quantitative idea, we calculated the area under the curve of Fig. 9(b) for pore sizes > 8 Å. For the **RO** process, the area under the curve of Fig. 9(b) for pore sizes > 8 Å is 23% *larger* than for **RO+E** process. In contrast to the 3% case, with the application of external electric field, water permeance through layered GO membrane increases for the 10% case. As can be seen from Fig. 10, for the case of 10% water dissociation, there is an overall increase in the number of larger pores (> 7.5 Å) for layered GO membrane under the influence of external electric field. For the **RO** process, the area under the curve of Fig. 10(b) for pore sizes > 7.5 Å is 16% *lower* than for the **RO+E** process!

The above observed different behavior of the 3% and the 10% cases under external electric field can be attributed to the dynamics of H_3O^+/OH^- ions. As one can see from Figs. 11(a) and 11(b), under the influence of external electric field, the H_3O^+/OH^- ions become more diffusive for the case of 3% water dissociation. This could also be observed in the dynamics of the H_3O^+/OH^- ions for the 3% case as reported in the supporting information (Figs. S11 and S12). Because of this, the size of the clusters reduces and consequently, the number of larger pores for **RO+E** decreases as compared to **RO**. On the other hand, the effect of external electric field on the diffusivity of H_3O^+/OH^- ions is almost negligible for the 10% case, as can be seen from Figs. 11(a) and 11(b). The dynamics of the H_3O^+/OH^- ions for

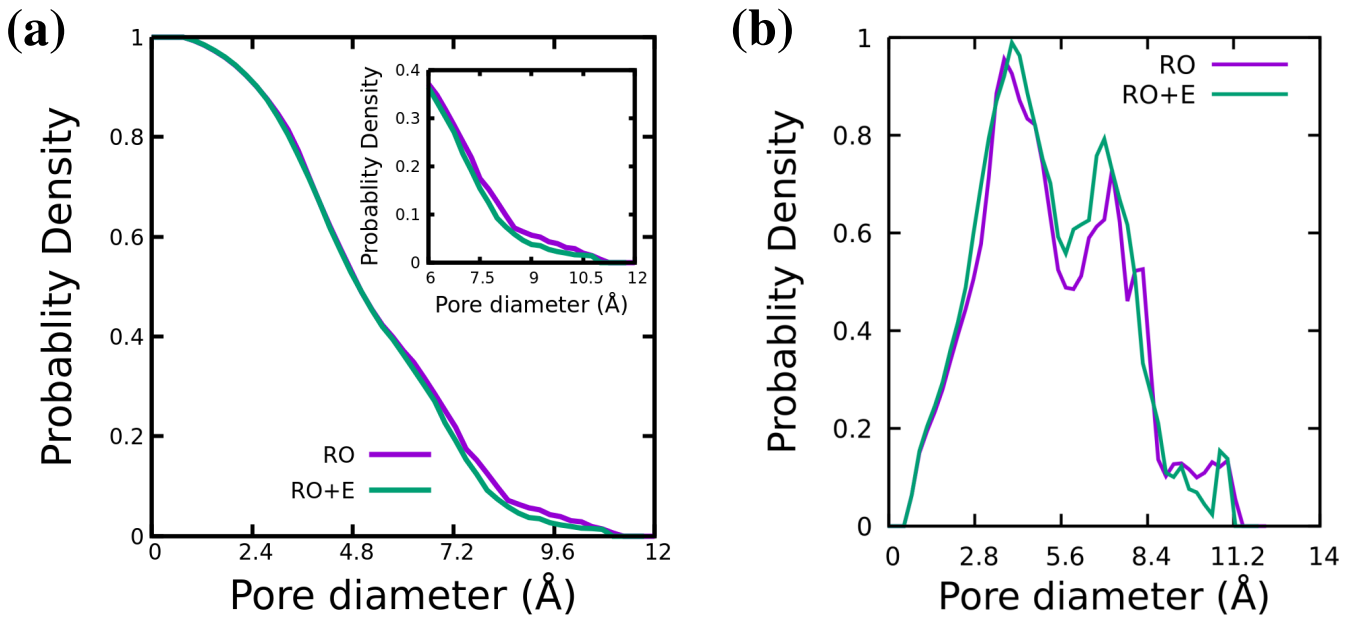

Figure 9: (a) $C(D)$, (b) PSD for the 3% case considering clustering of H_3O^+/OH^- ions.

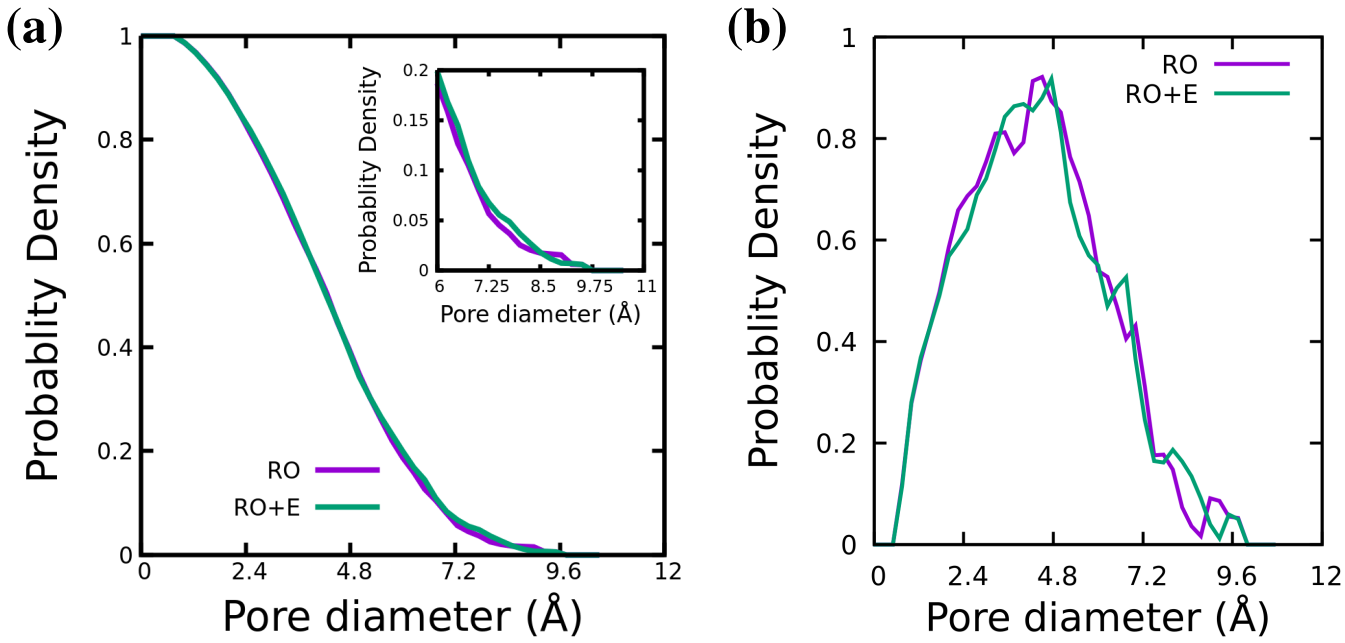

Figure 10: (a) $C(D)$, (b) PSD for the 10% case considering clustering of H_3O^+/OH^- ions.

the 10% case also reveals the same (Figs. S13 and S14 of the supporting information). This is due to the fact that for the 10% case, the H_3O^+/OH^- ions form larger clusters, lacking space for motion inside the interlayer gallery of the layered GO membranes. However, the electric field causes an overall increase in the larger pore sizes (> 7.5 Å) in the layered GO membranes because of the fluctuations of the GO nanosheets. This causes more water permeance for the 10% case under the influence of external electric field. Also, because of the smaller size of the Na^+ ion compared to the Cl^- ions, this increase in the larger pore sizes also affects the intercalation of Na^+ ions inside the membrane - as seen in Fig. 7(b). With the application of external electric field, more Na^+ ions get intercalated inside the membrane for the 10% case,

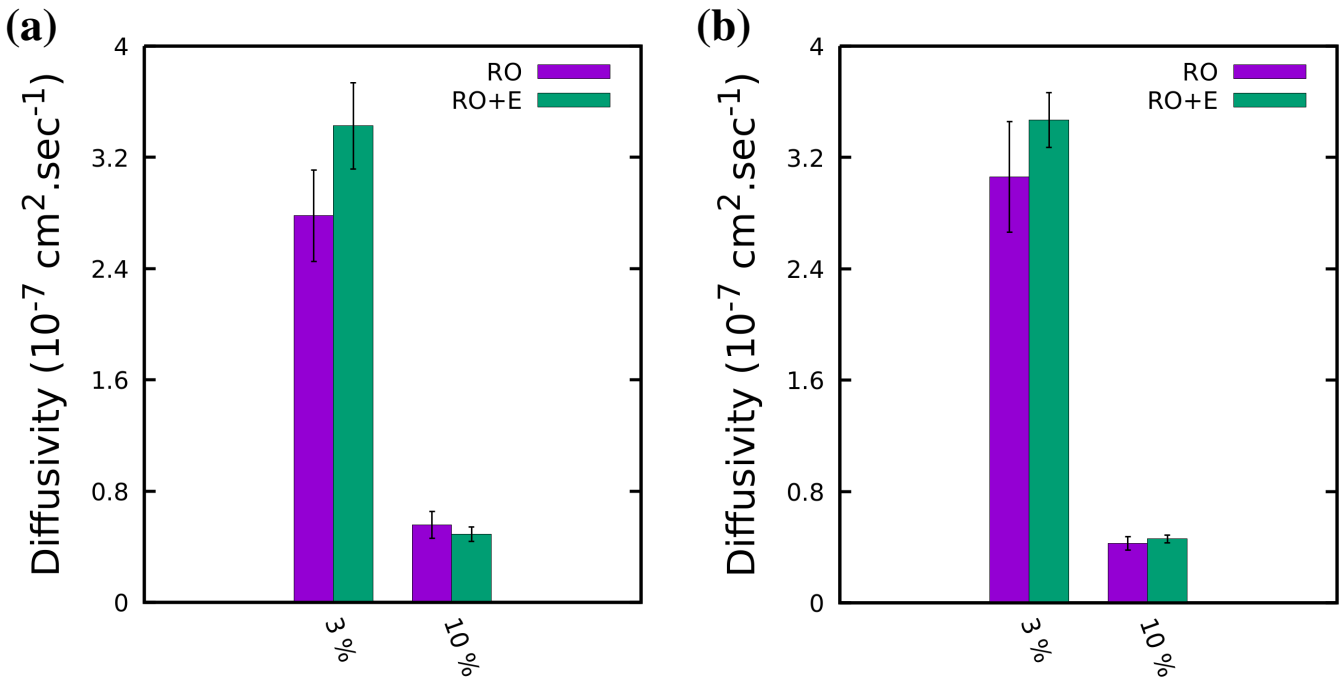

Figure 11: Diffusivity of (a) H_3O^+ ions and (b) OH^- ions inside the interlayer gallery of layered GO membranes.

even though the external electric field is applied along the $-Z$ direction (i.e. from feed solution to the permeate side).

4 Conclusions

We analyzed in detail, the performance of layered GO membrane under the influence of an external oscillating electric field, considering a modest amount of dissociation of water molecules into H_3O^+/OH^- ions. The dissociation of water molecules inside the interlayer gallery of layered GO membrane decreases the water permeance through the membrane. Here, two factors play important role: 1) clustering of H_3O^+/OH^- ions, and 2) increase in the stability of the H-bond network between water molecules and the GO nanosheets in the presence of H_3O^+/OH^- ions. The clustering of H_3O^+/OH^- ions also impedes the permeation of salt ions through the layered GO membranes. We attribute the increase in the stability of H-bond network between water molecules and the GO nanosheets to the slow water orientational relaxation dynamics ($\mathbf{C_e}$) inside the interlayer gallery of the membranes in the presence of H_3O^+/OH^- ions. Encouragingly, it is observed that the H_3O^+/OH^- ions impart stability to layered GO membranes in aqueous environment. This stems from the fact that water molecules located close to the H_3O^+/OH^- ions form stronger (or more stable) H-bond network with the GO nanosheets as compared to the water molecules located away from the H_3O^+/OH^- ions. This binding of the GO nanosheets becomes stronger as more water molecules get dissociated into H_3O^+/OH^- ions.

We further revealed that the dynamics of the H_3O^+/OH^- ions also influences the performance of the layered GO membranes. For small concentration of H_3O^+/OH^- ions (or low dissociation of water molecules), their dynamics is significantly affected by the external electric field, which in turn affects the performance of the membrane. As a continuation of this study, it is important to investigate the performance of the layered GO membrane under the influence of external electric field with different frequencies, amplitudes and applied directions. Along with this, GO nanosheets with different degree of partial reductions also could be considered. With such an outlook, the observations

reported in the present work provide significant insights into the construction and tailoring of pragmatic GO membranes for various applications.

Acknowledgement

This work was supported by Research Foundation Flanders (FWO-Vl). The computational resources used in this work were provided by the VSC (Flemish Supercomputer Center) which is funded by Research Foundation Flanders and the Flemish Government department EWI.

Supporting Information

Clustering of H_3O^+/OH^- ions, Dynamics of H-bond between water and GO nanosheets, Water orientational relaxation dynamics ($\mathbf{C_e}$), Pore size distribution, Pore size distribution considering the clustering of the H_3O^+/OH^- ions, Influence of stability in H-bonding between water molecules and GO nanosheets on the salt rejection, Dynamics of H_3O^+/OH^- ions, Influence of the frequency of the external electric field on the water orientational relaxation dynamics ($\mathbf{C_e}$), Water flux and salt rejection.

References

(1) Tanugi, D. C.; Grossman, J. C. Water Desalination across Nanoporous Graphene. *Nano Lett.* **2012**, *12*, 3602–3608.

(2) Tanugi, D. C.; Lin, L. C.; Grossman, J. C. Multilayer Nanoporous Graphene Membranes for Water Desalination. *Nano Lett.* **2016**, *16*, 1027–1033.

(3) Das, R.; Ali, M. E.; Hamid, S. B. A.; Ramakrishna, S.; Chowdhury, Z. Z. Carbon Nanotube Membranes for Water Purification: A Bright Future in Water Desalination. *Desalination* **2014**, *336*, 97–109.

(4) Joshi, R. K.; Carbone, P.; Wang, F. C.; Kravets, V. G.; Su, Y.; Grigorieva, I. V.; Wu, H. A.; Geim, A. K.; Nair, R. R. Precise and Ultrafast Molecular Sieving Through Graphene Oxide Membranes. *Science* **2014**, *343*, 752–754.

(5) Nair, R. R.; Wu, H. A.; Jayaram, P. N.; Grigorieva, I. V.; Geim, A. K. Unimpeded Permeation of Water Through Helium-Leak-Tight Graphene-Based Membranes. *Science* **2012**, *335*, 442–444.

(6) Wei, N.; Peng, X.; Xu, Z. Understanding Water Permeation in Graphene Oxide Membranes. *ACS Appl. Mater. Interfaces* **2014**, *6*, 5877–5883.

(7) Surwade, S. P.; Smirnov, S. N.; Vlassiouk, I. V.; Unocic, R. R.; Veith, G. M.; Dai, S.; Mahurin, S. M. Water Desalination using Nanoporous Single-Layer Graphene. *Nat. Nanotechnol.* **2015**, *10*, 459–464.

(8) Seo, D. H.; Pineda, S.; Woo, Y. C.; Xie, M.; Murdock, A. T.; Ang, E. Y. M.; Jiao, Y.; Park, M. J.; Lim, S. I.; Lawn, M.; Borghi, F. F.; Han, Z. J.; Gray, S.; Millar, G.; Du, A.; Shon, H. K.; Ng, T. Y.; Ostrikov, K. K. Anti-Fouling Graphene-Based Membranes for Effective Water Desalination. *Nat. Commun.* **2018**, *9*, 683.

(9) Anichini, C.; Aliprandi, A.; Gali, S. M.; Liscio, F.; Morandi, V.; Minoia, A.; Beljonne, D.; Ciesielski, A.; Samorì, P. Ultrafast and Highly Sensitive Chemically Functionalized Graphene Oxide-Based Humidity Sensors: Harnessing Device Performances via the Supramolecular Approach. *ACS Appl. Mater. Interfaces* **2020**, *12*, 44017–44025.

(10) Ahmed, A.; Adak, B.; Bansala, T.; Mukhopadhyay, S. Green Solvent Processed Cellulose/Graphene Oxide Nanocomposite Films with Superior Mechanical, Thermal, and Ultraviolet Shielding Properties. *ACS Appl. Mater. Interfaces* **2020**, *12*, 1687–1697.

(11) Yun, J.; Echols, I.; Flouda, P.; Chen, Y.; Wang, S.; Zhao, X.; Holta, D.;

Radovic, M.; Green, M. J.; Naraghi, M.; Lutkenhaus, J. L. Layer-by-Layer Assembly of Reduced Graphene Oxide and MXene Nanosheets for Wire-Shaped Flexible Supercapacitors. *ACS Appl. Mater. Interfaces* **2021**, *13*, 14068–14076.

(12) Song, W.; Chen, P.; Yan, J.; Zhu, W.; Ji, H. The Tribological Properties of Reduced Graphene Oxide Doped by N and B Species with Different Configurations. *ACS Appl. Mater. Interfaces* **2020**, *12*, 29737–29746.

(13) Jang, J.; Song, S. H.; Kim, H.; Moon, J.; Ahn, H.; Jo, K.-I.; Bang, J.; Kim, H.; Koo, J. Janus Graphene Oxide Sheets with Fe_3O_4 Nanoparticles and Polydopamine as Anodes for Lithium-Ion Batteries. *ACS Appl. Mater. Interfaces* **2021**, *13*, 14786–14795.

(14) Han, Y.; Jiang, Y.; Gao, C. High-Flux Graphene Oxide Nanofiltration Membrane Intercalated by Carbon Nanotubes. *ACS Appl. Mater. Interfaces* **2015**, *7*, 8147–8155.

(15) Huang, H.-H.; Joshi, R. K.; De Silva, K. K. H.; Badam, R.; Yoshimura, M. Fabrication of Reduced Graphene Oxide Membranes for Water Desalination. *J. Membr. Sci.* **2019**, *572*, 12–19.

(16) Padmavathy, N.; Behera, S. S.; Pathan, S.; Das Ghosh, L.; Bose, S. Interlocked Graphene Oxide Provides Narrow Channels for Effective Water Desalination through Forward Osmosis. *ACS Appl. Mater. Interfaces* **2019**, *11*, 7566–7575.

(17) Zhang, Y.; Zhang, S.; Gao, J.; Chung, T.-S. Layer-by-Layer Construction of Graphene Oxide (GO) Framework Composite Membranes for Highly Efficient Heavy Metal Removal. *J. Membr. Sci.* **2016**, *515*, 230–237.

(18) Mohammadi, A.; Daymond, M. R.; Docoslis, A. Graphene Oxide Membranes for Isotopic Water Mixture Filtration: Preparation, Physicochemical Characterization, and Performance Assessment. *ACS Appl. Mater. Interfaces* **2020**, *12*, 34736–34745.

(19) Yu, P.; Xiong, Z.; Zhan, H.; Xie, K.; Zhong, Y. L.; Simon, G. P.; Li, D. Electrochemically-Derived Graphene Oxide Membranes with High Stability and Superior Ionic Sieving. *Chem. Commun.* **2019**, *55*, 4075–4078.

(20) Abraham, J.; Vasu, K. S.; Williams, C. D.; Gopinadhan, K.; Su, Y.; Cherian, C. T.; Dix, J.; Prestat, E.; Haigh, S. J.; Grigorieva, I. V.; Carbone, P.; Geim, A. K.; Nair, R. R. Tunable Sieving of Ions using Graphene Oxide Membranes. *Nat. Nanotechnol.* **2017**, *12*, 546–550.

(21) Dou, H.; Xu, M.; Jiang, B.; Wen, G.; Zhao, L.; Wang, B.; Yu, A.; Bai, Z.; Sun, Y.; Zhang, L.; Chen, Z.; Jiang, Z. Bioinspired Graphene Oxide Membranes with Dual Transport Mechanisms for Precise Molecular Separation. *Adv. Funct. Mater.* **2019**, *29*, 1905229.

(22) Peng, C.; Iqbal, Z.; Sirkar, K. K.; Peterson, G. W. Graphene Oxide-Based Membrane as a Protective Barrier against Toxic Vapors and Gases. *ACS Appl. Mater. Interfaces* **2020**, *12*, 11094–11103.

(23) Liu, Q.; Gupta, K. M.; Xu, Q.; Liu, G.; Jin, W. Gas Permeation through Double-Layer Graphene Oxide Membranes: The Role of Interlayer Distance and Pore Offset. *Sep. Purif. Technol.* **2019**, *209*, 419–425.

(24) Lee, H.-Y.; Heish, Y.-C.; Lee, C.-T. High Sensitivity Detection of Nitrogen Oxide Gas at Room Temperature using Zinc Oxide-Reduced Graphene Oxide Sensing Membrane. *J. Alloys Compd.* **2019**, *773*, 950–954.

(25) Talyzin, A. V.; Hausmaninger, T.; You, S.; Szabó, T. The Structure of Graphene Oxide Membranes in Liquid Water, Ethanol

and Water-Ethanol Mixtures. *Nanoscale* **2014**, *6*, 272–281.

(26) Yeh, C. N.; Raidongia, K.; Shao, J.; Yang, Q. H.; Huang, J. On the Origin of the Stability of Graphene Oxide Membranes in Water. *Nat. Chem.* **2015**, *7*, 166–170.

(27) Williams, C. D.; Carbone, P.; Siperstein, F. R. In Silico Design and Characterization of Graphene Oxide Membranes with Variable Water Content and Flake Oxygen Content. *ACS Nano* **2019**, *13*, 2995–3004.

(28) Liu, H.; Wang, H.; Zhang, X. Facile Fabrication of Freestanding Ultrathin Reduced Graphene Oxide Membranes for Water Purification. *Adv. Mater.* **2015**, *27*, 249–254.

(29) Zhao, Z.; Ni, S.; Su, X.; Gao, Y.; Sun, X. Thermally Reduced Graphene Oxide Membrane with Ultrahigh Rejection of Metal Ions' Separation from Water. *ACS Sustainable Chem. Eng.* **2019**, *7*, 14874–14882.

(30) Jia, Z.; Wang, Y. Covalently Crosslinked Graphene Oxide Membranes by Esterification Reactions for Ions Separation. *J. Mater. Chem. A* **2015**, *3*, 4405–4412.

(31) Song, Y.; Li, R.; Pan, F.; He, Z.; Yang, H.; Li, Y.; Yang, L.; Wang, M.; Wang, H.; Jiang, Z. Ultrapermeable Graphene Oxide Membranes With Tunable Interlayer Distances via Vein-Like Supramolecular Dendrimers. *J. Mater. Chem. A* **2019**, *7*, 18642–18652.

(32) Huang, H.; Song, Z.; Wei, N.; Shi, L.; Mao, Y.; Ying, Y.; Sun, L.; Xu, Z.; Peng, X. Ultrafast Viscous Water Flow through Nanostrand-Channelled Graphene Oxide Membranes. *Nat. Commun.* **2013**, *4*, 1–9.

(33) Goh, K.; Jiang, W.; Karahan, H. E.; Zhai, S.; Wei, L.; Yu, D.; Fane, A. G.; Wang, R.; Chen, Y. All-Carbon Nanoarchitectures as High-Performance Separation Membranes with Superior Stability. *Adv. Funct. Mater.* **2015**, *25*, 7348–7359.

(34) ho Song, J.; Yu, H.-W.; Ham, M.-H.; Kim, I. S. Tunable Ion Sieving of Graphene Membranes through the Control of Nitrogen-Bonding Configuration. *Nano Lett.* **2018**, *18*, 5506–5513.

(35) Wu, W.; Su, J.; Jia, M.; Zhong, W.; Li, Z.; Li, W. Ultrastable Sandwich Graphene Oxide Hollow Fiber Membranes with Confined Interlayer Spacing. *J. Mater. Chem. A* **2019**, *7*, 13007–13011.

(36) Talyzin, A.; Solozhenko, V.; Kurakevych, O.; Szabó, T.; Dékány, I.; Kurnosov, A.; Dmitriev, V. Colossal Pressure-Induced Lattice Expansion of Graphite Oxide in the Presence of Water. *Angew. Chem. Int. Ed.* **2008**, *47*, 8268–8271.

(37) Wang, W.; Eftekhari, E.; Zhu, G.; Zhang, X.; Yan, Z.; Li, Q. Graphene Oxide Membranes with Tunable Permeability due to Embedded Carbon Dots. *Chem. Commun.* **2014**, *50*, 13089–13092.

(38) Xu, X. L.; Lin, F. W.; Du, Y.; Zhang, X.; Wu, J.; Xu, Z. K. Graphene Oxide Nanofiltration Membranes Stabilized by Cationic Porphyrin for High Salt Rejection. *ACS Appl. Mater. Interfaces* **2016**, *8*, 12588–12593.

(39) Zhang, Y.; Zhang, S.; Chung, T. S. Nanometric Graphene Oxide Framework Membranes with Enhanced Heavy Metal Removal via Nanofiltration. *Environ. Sci. Technol.* **2015**, *49*, 10235–10242.

(40) Perreault, F.; de Faria, A. F.; Elimelech, M. Environmental Applications of Graphene-Based Nanomaterials. *Chem. Soc. Rev.* **2015**, *44*, 5861–5896.

(41) Li, W.; Wu, W.; Li, Z. Controlling Interlayer Spacing of Graphene Oxide Mem-

branes by External Pressure Regulation. *ACS Nano* **2018**, *12*, 9309–9317.

(42) Hu, C.; Liu, Z.; Lu, X.; Sun, J.; Liu, H.; Qu, J. Enhancement of the Donnan Effect through Capacitive Ion Increase using an Electroconductive rGO-CNT Nanofiltration Membrane. *J. Mater. Chem. A* **2018**, *6*, 4737–4745.

(43) Chen, X.; Qiu, M.; Ding, H.; Fu, K.; Fan, Y. A Reduced Graphene Oxide Nanofiltration Membrane Intercalated by Well-Dispersed Carbon Nanotubes for Drinking Water Purification. *Nanoscale* **2016**, *8*, 5696–5705.

(44) Gao, S. J.; Qin, H.; Liu, P.; Jin, J. SWCNT-Intercalated GO Ultrathin Films for Ultrafast Separation of Molecules. *J. Mater. Chem. A* **2015**, *3*, 6649–6654.

(45) Chen, L.; Shi, G.; Shen, J.; Peng, B.; Zhang, B.; Wang, Y.; Bian, F.; Wang, J.; Li, D.; Qian, Z.; Xu, G.; Liu, G.; Zeng, J.; Zhang, L.; Yang, Y.; Zhou, G.; Wu, M.; Jin, W.; Li, J.; Fang, H. Ion Sieving in Graphene Oxide Membranes via Cationic Control of Interlayer Spacing. *Nature* **2017**, *550*, 380–383.

(46) Liang, S.; Wang, S.; Chen, L.; Fang, H. Controlling Interlayer Spacings of Graphene Oxide Membranes with Cationic for Precise Sieving of Mono-/Multi-Valent Ions. *Sep. Purif. Technol.* **2020**, *241*, 116738.

(47) Zhou, K.-G.; Vasu, K. S.; Cherian, C. T.; Neek-Amal, M.; Zhang, J. C.; G-Kalashami, H.; K. Huang, O. P. M.; Kravets, V. G.; Abraham, J.; Su, Y.; Grigorenko, A. N.; Pratt, A.; Geim, A. K.; Peeters, F. M.; Novoselov, K. S.; Nair, R. R. Electrically Controlled Water Permeation through Graphene Oxide Membranes. *Nature* **2018**, *559*, 236–240.

(48) Mortazavi, V.; Moosavi, A.; N.-Borujerdi, A. Enhancing Water Desalination in Graphene-based Membranes via an Oscillating Electric Field. *Desalination* **2020**, *495*, 114672.

(49) Zhang, H.; Liu, B.; Wu, M.-S.; Zhou, K.; Law, A. W.-K. Transport of Salty Water through Graphene Bilayer in an Electric Field: A Molecular Dynamics Study. *Comput. Mater. Sci.* **2017**, *131*, 100–107.

(50) Humphrey, W.; Dalke, A.; Schulten, K. VMD: Visual Molecular Dynamics. *J. Mol. Graphics* **1996**, *14*, 33–38.

(51) Hanwell, M. D.; Curtis, D. E.; Lonie, D. C.; Vandermeersch, T.; Zurek, E.; Hutchison, G. R. Avogadro: An Advanced Semantic Chemical Editor, Visualization, and Analysis Platform. *J. Cheminf.* **2012**, *4*, 1–17.

(52) Tang, H.; Liu, D.; Zhao, Y.; Yang, X.; Lu, J.; Cui, F. Molecular Dynamics Study of the Aggregation Process of Graphene Oxide in Water. *J. Phys. Chem. C* **2015**, *119*, 26712–26718.

(53) Shih, C. J.; Lin, S.; Sharma, R.; Strano, M. S.; Blankschtein, D. Understanding the pH-Dependent Behavior of Graphene Oxide Aqueous Solutions: A Comparative Experimental and Molecular Dynamics Simulation Study. *Langmuir* **2012**, *28*, 235–241.

(54) Gogoi, A.; Reddy, K. A.; Mondal, P. Multilayer Graphene Oxide Membrane in Forward Osmosis: Molecular Insights. *ACS Appl. Nano Mater.* **2018**, *1*, 4450–4460.

(55) Gogoi, A.; Konch, T. J.; Raidongia, K.; Reddy, K. A. Water and Salt Dynamics in Multilayer Graphene Oxide (GO) Membrane: Role of Lateral Sheet Dimensions. *J. Membr. Sci.* **2018**, *563*, 785–793.

(56) Gogoi, A.; Koneru, A.; Reddy, K. A. Effect of Graphene Oxide (GO) Nanosheet Sizes, Pinhole Defects and Non-Ideal Lamellar Stacking on the Performance of Layered GO Membranes: An Atomistic Investigation. *Nanoscale Adv.* **2019**, *1*, 3023–3035.

(57) K., V. P.; Kannam, S. K.; Hartkamp, R.; Sathian, S. P. Water Desalination using Graphene Nanopores: Influence of the Water Models used in Simulations. *Phys. Chem. Chem. Phys.* **2018**, *20*, 16005–16011.

(58) Akhavan, M.; Schofield, J.; Jalili, S. Water Transport and Desalination through Double-Layer Graphyne Membranes. *Phys. Chem. Chem. Phys.* **2018**, *20*, 13607–13615.

(59) Mahdizadeh, S. J.; Goharshadi, E. K.; Akhlamadi, G. Seawater Desalination using Pillared Graphene as a Novel Nano-Membrane in Reverse Osmosis Process: Nonequilibrium MD Simulation Study. *Phys. Chem. Chem. Phys.* **2018**, *20*, 22241–22248.

(60) Phillips, J. C.; Braun, R.; Wang, W.; Gumbart, J.; Tajkhorshid, E.; Villa, E.; Chipot, C.; D.Skeel, R.; Kalé, L.; Schulten, K. Scalable Molecular Dynamics with NAMD. *J. Comput. Chem.* **2005**, *26*, 1781–1802.

(61) Jorgensen, W. L.; Maxwell, D. S.; Rives, J. T. Development and Testing of the OPLS All-Atom Force Field on Conformational Energetics and Properties of Organic Liquids. *J. Am. Chem. Soc.* **1996**, *118*, 11225–11236.

(62) Jorgensen, W. L.; Chandrasekhar, J.; Madura, J. D.; Impey, R. W.; Klein, M. L. Comparison of Simple Potential Functions for Simulating Liquid Water. *J. Chem. Phys.* **1983**, *79*, 926–935.

(63) Miyamoto, S.; Kollman, P. A. Settle: An Analytical Version of the SHAKE and RATTLE Algorithm for Rigid Water Models. *J. Comput. Chem.* **1992**, *13*, 952–962.

(64) Essmann, U.; Perera, L.; Berkowitz, M. L.; Darden, T.; Lee, H.; ; Pedersen, L. G. A Smooth Particle Mesh Ewald Method. *J. Chem. Phys.* **1995**, *103*, 8577–8593.

(65) Rapaport, D. C. Hydrogen Bonds in Water Network Organization and Lifetimes. *Mol. Phys.* **1983**, *50*, 1151–1162.

(66) l. Yeh, Y.; Mou, C.-Y. Orientational Relaxation Dynamics of Liquid Water Studied by Molecular Dynamics Simulation. *J. Phys. Chem. B* **1999**, *103*, 3699–3705.

(67) Bhattacharya, S.; Gubbins, K. E. Fast Method for Computing Pore Size Distributions of Model Materials. *Langmuir* **2006**, *22*, 7726–7731.

For Table of Contents Only